Nanoscale

ROYAL SOCIETY OF CHEMISTRY

COMMUNICATION

View Article Online
View Journal | View Issue

Cite this: *Nanoscale*, 2021, **13**, 15215

Received 30th June 2021,
Accepted 30th August 2021

DOI: 10.1039/d1nr04229g

rsc.li/nanoscale

Power discontinuity and shift of the energy onset of a molecular de-bromination reaction induced by hot-electron tunneling†

Ana Barragán,[a,b,c] Roberto Robles, *[c] Nicolás Lorente[a,c] and Lucia Vitali *[a,b,c,d]

Understanding the mechanism of molecular dissociation under applied bias is a fundamental requirement to progress in (electro)-catalysis as well as in (opto)-electronics. The working conditions of a molecular-based device and the stability of chemical bonds can be addressed in metal–organic junctions by injecting electrons in tunneling conditions. Here, we have correlated the energy of de-bromination of an aryl group with its density of states in a self-assembled dimeric structure of 4′-bromo-4-mercaptobiphenyl adsorbed on a Au(111) surface. We have observed that the electron-energy range where the molecule is chemically stable can be extended, shifting the bias threshold for the rupture of the –C–Br bond continuously from about 2.4 to 4.4 V by changing the electron current. Correspondingly, the power needed for the dissociation drops sharply at 3.6 V, identifying different reaction regimes and the contribution of different molecular resonance states.

Hot-electron interaction with metal–organic structures is of paramount importance for the development of different systems including catalysis and nano-electronics. Regardless of the optical, thermal, or charge-injection origin of these electrons, they will rapidly be transported through the molecule or equilibrate to the Fermi level by exchanging energy with the system. The immediate, albeit transitory, electron occupation of well-defined molecular orbitals, or its energy exchange process, is beneficial for the activation of chemical reactions.[1–8] Paradoxically, the electron interaction itself constitutes one of the main limits to the structural stability of organics in (opto)-electronics.[9–13] Halide complexes are one example of these structures undergoing chemical changes. Indeed, de-halogenation process is at the base of polymeric synthesis and a possible cause of break-down of sensors and energy conversion systems during operation.[12,14–17] The molecular stability has been addressed so far focusing mainly either on their anchoring to metal electrodes, or on the alignment of the electronic properties of the system.[10–12,18] Despite efforts to promote the reaction or *vice versa*, the alleviating actions to prevent the molecular dissociation, so far it is unclear how to control the distinct reaction channels offered by the organics and the metal electrodes.

Here, we monitor the mechanisms undermining the physical–chemical robustness of halogen-functionalized molecules against electron injections. Specifically, we have studied the induced dissociation of the –C–Br bond of a 4′-bromo-4-mercaptobiphenyl, (hereafter Br-MBP) assembled in a metal–organic structure on Au(111) surface, by means of scanning-probe techniques at low temperature and density-functional-theory calculations. We report that the set point of the de-halogenation reaction can be tuned involving different electronic properties of the system from 2.4 to 4.4 V. As the onset of the dissociation shifts towards higher electron-energies, different molecular orbitals are involved. Correspondingly, the power needed for the detachment of the halogen atoms undergoes a sharp and abrupt discontinuity. A model considering the opening of multiple conductance channels is proposed to explain the experimental evidences.

The prototypical configuration of Br-MBP molecules adsorbed at room temperature on the Au(111) surface is shown in Fig. 1. The molecules adsorb along the [11$\bar{2}$] high-symmetry direction of Au(111) assembling in a metal–organic dimeric structure, namely Au(Br-MBP)$_2$. According to our DFT calculations, the dehydrogenated sulfhydryl group of the molecule, followed by the covalent binding of two molecules to one Au adatom in a S–Au–S bond, is the most energetically favorable configuration (Fig. 1b and ESI†), recalling the adsorption con-

[a]*Donostia International Physics Center (DIPC), Paseo M Lardizabal 4, 20018 San Sebastián, Spain. E-mail: lucia.vitali@ehu.es*
[b]*Advanced Polymers and Materials: Physics, Chemistry and Technology, Chemistry Faculty (UPV/EHU), Paseo M Lardizabal 3, 20018 San Sebastián, Spain*
[c]*Centro de Física de Materiales CFM/MPC(CSIC-UPV/EHU), Paseo M Lardizabal 5, 20018 San Sebastián, Spain. E-mail: roberto.robles@csic.es*
[d]*Ikerbasque Research Foundation for Science, Plaza Euskadi, 5, Bilbao 48009, Spain*

†Electronic supplementary information (ESI) available: Complementary experimental and theoretical results including methods, theoretical results on adsorption energetics and density of states, experimental manipulation of Au(Br-MBP)$_2$ complex. See DOI: 10.1039/d1nr04229g

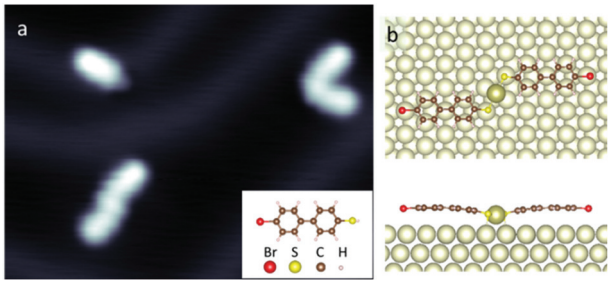

Fig. 1 Structural characterization. (a) Topographic image (8.2 nm × 11 nm) showing mono- or dimeric complexes formed upon deposition of the Br-MBP molecules (inset) on Au (111). *cis* ("V"shaped) and *trans* ("S"shaped) configurations can be observed. (b) Simulated structure of a Au (Br-MBP)$_2$ complex on the Au(111) surface.

figuration commonly accepted for thiols molecules on Au surfaces.[19–21] In this bonding configuration, the molecular backbone weakly interacts with the substrate, and it adsorbs in an almost planar and parallel configuration to the surface (Fig. 1b). The two *cis* ("V" shaped) and *trans* ("S"shaped) configurations of the Au(Br-MBP)$_2$ complex observed in Fig. 1 are energetically equivalent and favored over the isolated monomer by almost 300 meV according to our DFT calculations (ESI†).

Adsorption configuration, chemical bonding and interaction with the substrate are important parameters for understanding the electronic properties and reactivity of the injected tunnel electrons. The dI/dV spectra measured along the Au(Br-MBP)$_2$ main axis, are shown in Fig. 2 as color-scale representations. These plots show that the local density of states and the contribution of specific molecular orbitals varies in space and in energy, both in the occupied and empty states energy regions. Energy maps at constant energy and their comparison with the theoretical dI/dV maps, shown in panels e–j, provide an intuitive visualization of the density of states and of their spatial position along the adsorbed Au(Br-MBP)$_2$ molecular complex.

Focusing on the density of states of the –C–Br region, we have clearly identified occupied states at energies −1.9 and −2.1 V (panels i and j). The experimental search for the empty state at the Br terminations predicted at high positive bias triggers the molecular de-bromination reaction preventing its experimental imaging into energy maps at sample bias larger than 2.2 V. Thus, only its theoretical expectation can be shown in panel e. Despite the fragility of this halogen bond to the tunneling electrons, this antibonding orbital can be observed in the density of states using the following method.

We have characterized the injection of hot-electrons into a specific molecular position, as the –C–Br bond, by locating the tip of the STM on top of the molecular orbital to be probed, as indicated by the red dots in the topographic images of Fig. 3a and b. By ramping the applied sample bias from 1 V to higher voltages and return, a clear and sharp discontinuity can be observed in the tunnel current I, witnessing an abrupt and irreversible modification of the tunnel junction at a critical

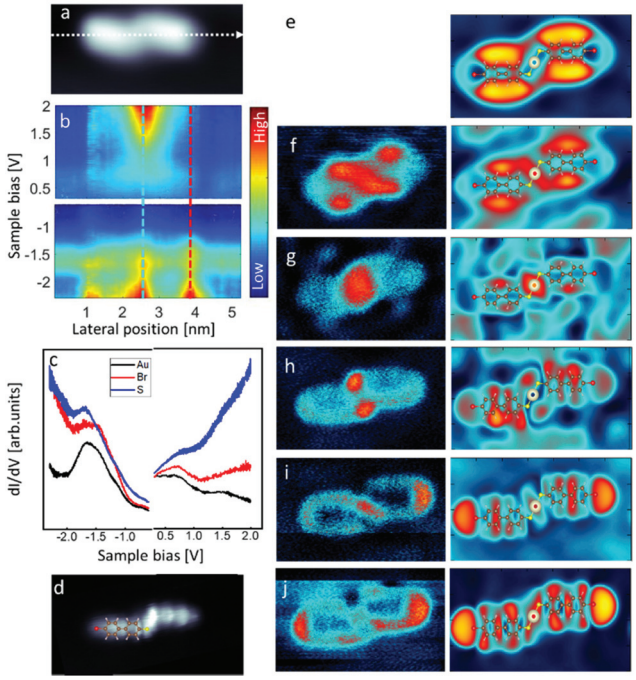

Fig. 2 Local electronic properties of the Au(Br-MBP)$_2$ complex. (a) Topographic image (5.2 nm × 2.4 nm). (b and c) Color-scale representation of 40 dI/dV spectra measured along the dotted line in panel a and selected dI/dV spectra at positions indicated in panel b. (d) Submolecular resolution of the Au(Br-MBP)$_2$ complex (e–j). Experimentally measured constant energy maps of the molecule (4 nm × 2.5 nm) at (e) 2.4 V; (f) 2 V; (g) 1.3 V; (h) −0.85 V; (i) −1.9 V; (j) −2.1 V and corresponding simulated maps with superposed molecular structure. (e) The experimental conductance map at 2.4 eV cannot be measured as scanning at this voltage causes the detachment of the Br atom.

voltage (red and light-red curves for the forward and backward directions in panel f, respectively). Subsequent topographic images (panels b and c) confirmed the detachment of the Br atom. This induced de-bromination reaction is irreversible and addressable on demand on each of the two Br atoms of the dimer, leading to equal results independently on the bromination state of the other edge of the molecule, or on the *cis* or *trans* configurations of the assembly. The topographic images show that the detached Br atoms are usually found apart from the MBP molecules, thus changing the electronic and structural configuration of the tunnel junction and explaining the discontinuity observed in the current. The de-brominated molecules preserve their adsorption configuration with respect to the high symmetry direction of Au(111), but bend towards the surface binding to a Au atom, as observed in the submolecular resolution image of Fig. 3d and confirmed by DFT calculations (panel e). The newly formed –C–Au bond is sufficiently strong to displace outwards the Au atom of the substrate partially reducing the molecular bending.

To shed some light on the bias-induced de-bromination reaction, we have repeated the measurement by locating the tip on top of the –C–Br region while increasing progressively

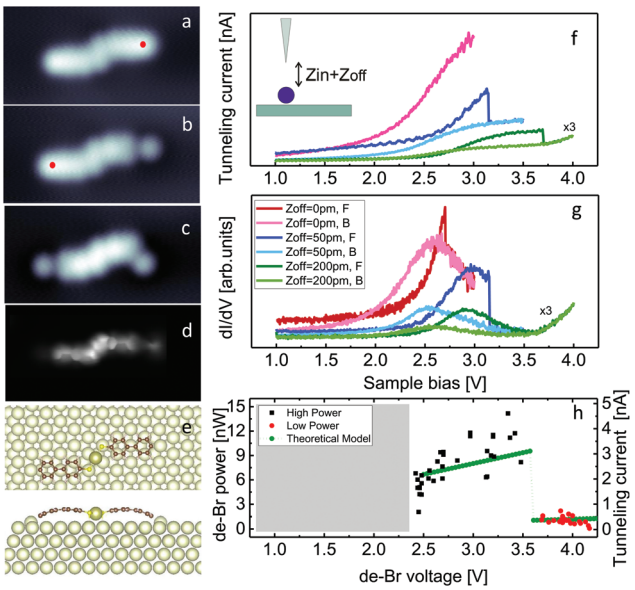

Fig. 3 Locally induced de-bromination reaction. (a–c) Chronological sequence of topographic images (5 nm × 2.5 nm). (d) Sub-molecular resolution of the $Au(MBP)_2$ dimer. (e) Adsorption configuration of the $Au(MBP)_2$ structure. (f) IV curves measured at variable tip–molecule distances Z_{offset}, at the positions indicated by the red dots in panels a and b. A sudden discontinuity shows the energy of de-bromination. The green curve is magnified by a factor 3. (g) Corresponding d*I*/d*V* spectra of the density of states before and after the de-bromination. (h) Reaction power. The green line is the result of a fit using a rate equation to estimate the reaction dynamics.

the tip–molecule distance adding defined vertical offsets Z_{offset}, thus reducing the tunnel current. It is worth stressing that in order to exclude artifacts caused by variation of the tip-ending configuration in the series of data, the applied vertical offset Z_{offset} has been selected in a random order. Similarly, tip artifacts have been further reduced by using the same initial set point of voltage and current (1 V, 0.7 nA) to preserve the fixed initial tip–sample distance Z_{in} in all dissociation measurements. Thus, even if Z_{in} is unknown, it contributes in the same way to the data and does not affect the conclusions.

In all measured cases, we observe that, by ramping the voltage according to the method described above, the critical voltage needed to induce the reaction shifts towards higher energies accordingly to the applied Z_{offset} (blue and green curves in Fig. 3f). As the dissociation reaction shifts towards higher energies, a molecular orbital is first outlined and then clearly visualized as a peak centered at about 2.9 V in the simultaneously measured d*I*/d*V* spectra (panel g). Once de-brominated, this molecular orbital is no more available, while a lower energy peak appears in the d*I*/d*V* spectrum at 2.5 V (*vide infra*). Thus, forward and backward d*I*/d*V* spectra survey the variation of the density of states induced by the reaction.

By plotting the observed de-bromination events according to their de-bromination voltage $V_{de\text{-}Br}$ and power $P_{de\text{-}Br}$, being $P_{de\text{-}Br} = I_{de\text{-}Br} \times V_{de\text{-}Br}$ (panel h), we observe that: (i) The de-bromination reaction occurs above a critical threshold voltage of 2.3 V, below which no reaction is observed neither at tunnel current up to 100 nA (grey area in the graph). The minimal de-bromination threshold voltage coincides with the onset of a molecular orbital. (ii) The chemical stability of the tunnel junction can be tuned, shifting continuously the de-bromination from the molecular orbital onset at 2.4 V to 4.4 V. The later value reflects the limit of our electronics to observe a sudden discontinuity in the current trace below 10 pA. (iii) The power needed to trigger the reaction increases progressively with the increasing voltage up to 3.6 V (black dots). Above 3.6 V, the reaction power shows an abrupt and sharp discontinuity. The power requested for the dissociation reduces from about 10 nW to roughly 2 nW (red dots). Additionally, in the large majority of cases, in this low-power regime the tunneling leads to double de-halogenation events, detaching the Br atoms from both sides of the $Au(Br\text{-}MBP)_2$ complex. Thus, the electron tunneling causes the de-bromination reaction also in the halogen termination not directly addressed by the tip of the STM. It is worth noting that DFT calculations predict a molecular orbital centered at the Br atom at 3.4 V (Fig. SI5†). Given the known underestimation of the energy of unoccupied states of DFT, this molecular resonance might be expected at an energy well above 3.6 V, thus in a region of the spectra dominated by the onset of the bulk state of the Au(111) (Fig. SI5†). The hybridization of this molecular state and the strong d*I*/d*V* signal of the substrate could explain its difficult observation in the experimental spectra. Thus, above 3.6 V, two distinct electronic states of Br trigger the reaction (*vide infra*).

Upon dissociation of Br, the charge density is rearranged in the molecular plane but no substantial charge transfer to the substrate occurs (Fig. SI3†). For clarity, in Fig. 4, the detached Br atoms have been displaced out of the scan range by manipulation with the tip of the microscope. The direct comparison of panel b of Fig. 2 and 4 provides already a very intuitive picture of the change in the density of states upon de-bromination of the dimer. As expected, the major change, both in the empty and in the occupied density of states, affects mainly the former –C–Br region where a –C–Au bond forms. The density of states at this position has a higher intensity than the one of the S–Au–S region at 1.3 V, which is almost unmodified by the reaction as seen in the maps at constant energy (panels e–k).

Based on the described phenomenological observations, we can assume that the trend in the de-bromination-power reflects the involved molecular states. Electron-induced molecular dissociation are usually explained by considering either the electron population of antibonding states or current-induced heating of vibrational modes.[3–5,9,13,18,21–24] However, in case of population of antibonding states, the electron-induced dissociation mechanism seems to largely dominate over the local heating.[4,13] Despite this, the described sharp drop of the reaction power shown in Fig. 3 needs more accurate considerations. Indeed, in order to reproduce the experimental evidences, we need to model the de-bromination dynamics considering the contribution of two molecular resonances. The different energies, at which these conductance

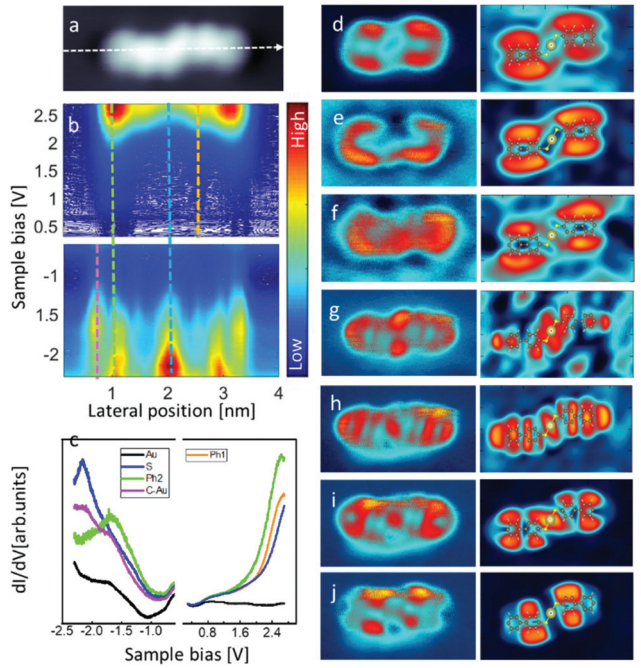

Fig. 4 Local electronic properties of the $Au(MBP)_2$ complex on Au(111). (a) Topographic image (3.9 nm × 1.6 nm). (b and c) Color-scale representation of 35 d*I*/d*V* spectra measured along the dotted line on panel a and selected spectra at positions marked in panel (b). (d–j). Comparison of the experimentally measured constant energy maps of the molecule (4 nm × 2.5 nm) at energies (d) 2.5 V; (e) 2 V; (f) 1.3 V; (g) −0.85 V; (h) −1.6 V; (i) −1.9 V; (j) −2.3 V and corresponding simulated maps.

channels open, allow a good fitting of the experimental data (green line in Fig. 3h and SI5–6†) and provide a simple explanation of the unexpected power discontinuity. Each of the two conductance channels brings in a new reaction path, thus increasing the probability of Br dissociation and dropping the power needed for the reaction. The size of the power drop and the values of the two slopes of the power with bias are univocally related. Indeed, it is impossible to change the relation between the slopes without changing the value of the power drop. This is an important constraint that, given the good agreement, lends extra weight to our interpretation of a second reaction channel opening at 3.6 V. It is worth noting that the sudden drop in the power above 3.6 V is due to the very effective contribution of the molecular state which is likely enhanced by its coupling strength and stronger hybridization with the bulk states of Au(111).[13]

Conclusions

In conclusion, we have described the electron induced dissociation of Br atom from the self-assembled $Au(Br\text{-}MBP)_2$ complex on Au(111) and its correlation with the density of states of the system. We have demonstrated that the energy range in which the molecule is chemically stable can be extended of almost 2 V. Correspondingly, the power needed for the de-bromination reaction undergoes a clear discontinuity reflecting the different molecular resonances involved. The identification of the parameters controlling the structural chemical stability of the metal–organic system constitutes one of the major outcomes of this work. This offers interesting prospects for heterogeneous catalysis, or for increased stability of the molecular components in organic electronics, and optoelectronic devices including energy conversion systems dealing with the injection or excitations of electrons above 2 V.

Conflicts of interest

There are no conflicts to declare.

Acknowledgements

A.B. acknowledges Vicerrectorado de Investigacion of the University of the Basque Country (UPV/EHU) for the PhD fellowship (2016). R.R. and N.L. are grateful for the computer resources at Finisterrae II, the technical support provided by CESGA and the EU-FET Open H2020 Mechanics with Molecules project (grant 766864). A.B. and L.V. acknowledge the funding of Spanish Ministry of Economy, Industry and Competitiveness (MINECO Grant number MAT2016-78293-C6-5-R); Diputacion Foral de Guipuzcoa (Red/Sarea 2020-CIEN-000009-01), and the Basque Government (Proyectos de Investigación Básica y/o Aplicada grant number PIBA-2021-0026).

Notes and references

1 Y.-J. Liu, P. Persson, H. O. Karlsson, S. Lunell, M. Kadi, D. Karlsson and J. Davidsson, *J. Chem. Phys.*, 2004, **120**, 6502–6509.
2 S. Linic, U. Aslam, C. Boerigter and M. Morabito, *Nat. Mater.*, 2015, **14**, 567–576.
3 S.-W. Hla, L. Bartels, G. Meyer and K.-H. Rieder, *Phys. Rev. Lett.*, 2000, **85**, 2777–2780.
4 L. Leung, T. Lim, Z. Ning and J. C. Polanyi, *J. Am. Chem. Soc.*, 2012, **134**, 9320–9326.
5 R. Ohmann, L. Vitali and K. Kern, *Nano Lett.*, 2010, **10**, 2995–3000.
6 M. Bonn, S. Funk, Ch. Hess, D. N. Denzel, C. Stampfl, M. Scheffler, M. Wolf and G. Ertl, *Science*, 1999, **285**(5430), 1042–1045.
7 M. F. Camellone, A. Correa, A. Barragan, M. Pedio, S. Fabris, C. Cepek and L. Vitali, *J. Phys. Chem. C*, 2019, **123**(11), 6496–6501.
8 G. J. Szulczewski and J. M. W hite, *Surf. Sci.*, 1998, **399**, 305–315.
9 A. Pecchia, G. Romano and A. Di Carlo, *Phys. Rev. B: Condens. Matter Mater. Phys.*, 2007, **75**, 035401.
10 G. Foti and H. Vazquez, *J. Phys. Chem. C.*, 2017, **121**, 1082–1088.

11 H. Li, T. A. Su, V. Zhang, M. L. Steigerwald, C. Nuckolls and L. Venkataraman, *J. Am. Chem. Soc.*, 2015, **137**, 5028–5033.
12 R. L. Starr, T. Fu, E. A. Doud, I. Stone, X. Roy and L. Venkataraman, *J. Am. Chem. Soc.*, 2020, **142**, 7128–7133.
13 A. Erpenbeck, Y. Ye, U. Peskin and M. Thoss, *Phys. Rev. B*, 2020, **102**, 195421.
14 L. Dong, P. N. Liu and N. Lin, *Acc. Chem. Res.*, 2015, **48**, 2765–2774.
15 A. Sarasola, A. Barragán and L. Vitali, *J. Am. Chem. Soc.*, 2018, **140**(46), 15631–15634.
16 A. Barragán, A. Sarasola and L. Vitali, *Angew. Chem.*, 2020, **59**, 15599–15602.
17 P. V. Kamat and M. Kunu, *Acc. Chem. Res.*, 2021, **54**, 520–531.
18 G. Schulze, K. J. Franke, A. Gagliardi, G. Romano, C. S. Lin, A. L. Rosa, T. A. Niehaus, Th. Frauenheim, A. Di Carlo, A. Pecchia and J. I. Pascual, *Phys. Rev. Lett.*, 2008, **100**, 136801.
19 P. Maksymovych and J. T. Yates Jr., *J. Am. Chem. Soc.*, 2008, **130**, 7518–7519.
20 P. Maksymovych, D. C. Sorescu and J. T. Yates Jr., *Phys. Rev. Lett.*, 2006, **97**, 146103.
21 C. Vericat, M. E. Vela, G. Benitez, P. Carro and R. C. Salvarezza, *Chem. Soc. Rev.*, 2010, **39**, 1805.
22 J. I. Pascual, N. Lorente, Z. Song, H. Conrad and H.-P. Rust, *Nature*, 2003, **423**, 525–528.
23 B. C. Stipe, M. A. Rezaei, W. Ho, S. Gao, M. Persson and B. I. Lundqvist, *Phys. Rev. Lett.*, 1997, **78**, 4410.
24 S. Mukherjee, F. Libisch, N. Large, O. Neumann, L. V. Brown, J. Cheng, J. B. Lassiter, E. A. Carter, P. Nordlander and N. J. Halas, *Nano Lett.*, 2013, **13**, 240.